Journal of Power Sources 256 (2014) 226–232

Contents lists available at ScienceDirect

Journal of Power Sources

journal homepage: www.elsevier.com/locate/jpowsour

Electrochemical impedance analysis of electrodeposited Si–O–C composite thick film on Cu microcones-arrayed current collector for lithium ion battery anode

Tao Hang [a,b], Daikichi Mukoyama [a], Hiroki Nara [a], Tokihiko Yokoshima [a], Toshiyuki Momma [a], Ming Li [b], Tetsuya Osaka [a,*]

[a] Research Institute for Science and Engineering, Waseda University, 3-4-1 Okubo, Shinjuku, Tokyo 169-8555, Japan
[b] School of Material Science and Engineering, Shanghai Jiao Tong University, 800 Dongchuan Rd., Shanghai 200240, PR China

HIGHLIGHTS

- The impedance of Si–O–C anode was investigated to understand its high performances.
- Wide range impedance spectroscopy was interpreted by a proposed equivalent circuit.
- Charge transfer resistance is main contribution to total resistance during discharge.
- The capacity fading is caused by SEI growth and increase of the electrode density.

GRAPHICAL ABSTRACT

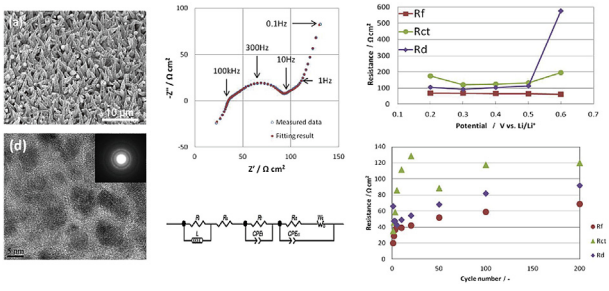

ARTICLE INFO

Article history:
Received 26 September 2013
Received in revised form
13 January 2014
Accepted 14 January 2014
Available online 24 January 2014

Keywords:
Electrochemical impedance spectrum
Si anode
Electrodeposition
Thick film
Lithium battery

ABSTRACT

The impedance behaviors of Si–O–C composite film electrodeposited on Cu microcones-arrayed current collector have been investigated to understand the electrochemical process kinetics that influences the cycling performance when used as a highly-durable anode in a lithium battery. The impedance was measured by using impedance spectroscopy in equilibrium conditions at various depths of discharge and during several hundred charge–discharge cycles. The measured impedance was interpreted with an equivalent circuit composed of solid electrolyte interphase (SEI) film, charge transfer and solid state diffusion. The impedance analysis shows that the change of charge transfer resistance is the main contribution to the total resistance change during discharge, but an abrupt augmentation of diffusive resistance at high depth of discharge is also observed which cannot be explained very well by the presented model. The impedance evolution of this electrode during charge–discharge cycles suggests that the slow growth of the SEI film as well as the increase of the electrode density are responsible for the capacity fading after long term cycling.

1. Introduction

Due to the demands of Li batteries with higher storage capacity and longer cycling life for applications such as implantable medical devices and next-generation electrical vehicles, it is very essential to develop new electrode materials with higher specific capacities [1–3]. Among all the materials proposed to replace graphite as the anode, silicon has been considered as one of the most promising

* Corresponding author. Department of Applied Chemistry, School of Advanced Science and Engineering, Faculty of Science and Engineering, Waseda University, 3-4-1 Okubo, Shinjuku-ku, Tokyo 169-8555, Japan. Tel.: +81 3 5286 3202; fax: +81 3 3205 2074.
E-mail address: osakatets@waseda.jp (T. Osaka).

0378-7753/$ – see front matter © 2014 Elsevier B.V. All rights reserved.
http://dx.doi.org/10.1016/j.jpowsour.2014.01.065

materials owing to its high theoretical specific capacity (4200 mAh g^{-1}), high volumetric capacity (9786 mAh cm^{-3}), and low charge/discharge voltage [4–6]. There are a number of studies on silicon-based electrodes including, micrometer, submicro meter, and nanosized particles, and various composite anodes [7–10]. However, all of these silicon-based materials experience a large inherent volume change during the lithiation and delithiation process, which leads to severe silicon particle pulverization and loss of electric contact with the current collector [11,12]. This mechanical disintegration and electronic degradation thereby triggered drastic capacity fading which is the main reason preventing commercial application of silicon in lithium ion secondary systems.

Recently, we have developed a novel Si–O–C composite thick film anode for Li battery by electrodeposition from an organic solvent with a complex structure current collector [13]. The electrodeposition method was introduced based on the assumption that, to form a Si containing anode from an organic solution, the composite of Si with an organic/inorganic compound withstands the stress during the anode operation [14]. This film, several microns thick, performed as a Li battery anode with a discharge (hereafter, discharge is defined as delithiation of the Si–O–C anode) capacity of ca. 1000 mAh g^{-1} of Si at 100 cycle and ca. 800 mAh g^{-1} even at 1000 cycle, which substantially improved electrochemical performance both in specific capacity and cycle ability [15]. Furthermore, a systematic study on the structural and chemical features was conducted by STEM, EELS, and XPS analyses to investigate the mechanism behind the cyclability enhancement of this unique Si–O–C anode. The buffering effect of the volume change was considered to be achieved by the formation of Li_2O, Li_2CO_3, and Li_4SiO_4. The main reactions related to the capacity of the silicon-based anode were considered to be the reaction from Si and SiO_2 to Li_xSi and $Li_2Si_2O_5$ [16]. Nevertheless, it's still necessary to make further efforts to understand the correlation between its structural change and electrochemical performance during charge–discharge cycles.

Electrochemical impedance spectroscopy (EIS) is a powerful tool to study the electrochemical behaviors occurring in the electrodes of Li-ion batteries. The resistance due to each kinetic step during the electrochemical reaction in the electrode can be obtained by this technique if the time constants are resolvable. Therefore, the evolution of the electrochemical and physical properties of the electrodes can be inferred from EIS data [17]. Various anode materials have been studied by EIS, such as carbon and Sn-based materials [18,19], using models to describe the total impedance of the electrode as the sum of the resistance and the capacitance of the solid electrolyte interphase (SEI) layer, the charge transfer resistance of the intercalation process, the double layer capacitance across the interface, and the solid state diffusion in the active materials. There are only a few reports devoted to investigating the impedance in silicon based materials, including the phase transformation and structural change of carbon-coated Si particles and Si nanowires [20–23], the formation of the SEI on Si thin film electrodes [24], and cyclability study of Si–C composite [17]. However, due to the unique structure of our electrodeposited Si–O–C composite anode supported by microcones array current collector, the reaction kinetics and mechanism of capacity fading during cycling may not be the same as the other Si anode reported before. In this work, the impedance behaviors of this unique structured Si–O–C composite anode at different depths of discharge (DOD) during the cycling process were systematically investigated in order to better understand the electrochemical kinetics and mechanism of capacity fading of the electrode.

2. Experimental

The Cu microcone-arrays current collectors were obtained by the electroless deposition method [25]. Commercial pure Cu foils after pretreatment were used as the substrate for the electroless deposition of microcone-arrays. The deposition electrolyte was composed of analytical pure $CuSO_4 \cdot 5H_2O$ (0.03 mol dm^{-3}), $NiSO_4 \cdot 6H_2O$ (0.0024 mol dm^{-3}), $NaH_2PO_2 \cdot H_2O$ (0.24 mol dm^{-3}), $Na_3C_6H_5O_7 \cdot 2H_2O$ (0.05 mol dm^{-3}) and H_3BO_3 (0.50 mol dm^{-3}) as well as crystallization modifier polyethylene glycol (5 ppm), dissolved in deionized water. The electroless deposition was performed for 20 min at pH 7.5–9.5 (adjusted by NaOH solution) and solution temperature of 65 °C. Subsequently, the Cu microcone-arrays substrates were rinsed with distilled water, dried in vacuum overnight, and transferred into an Ar atmosphere.

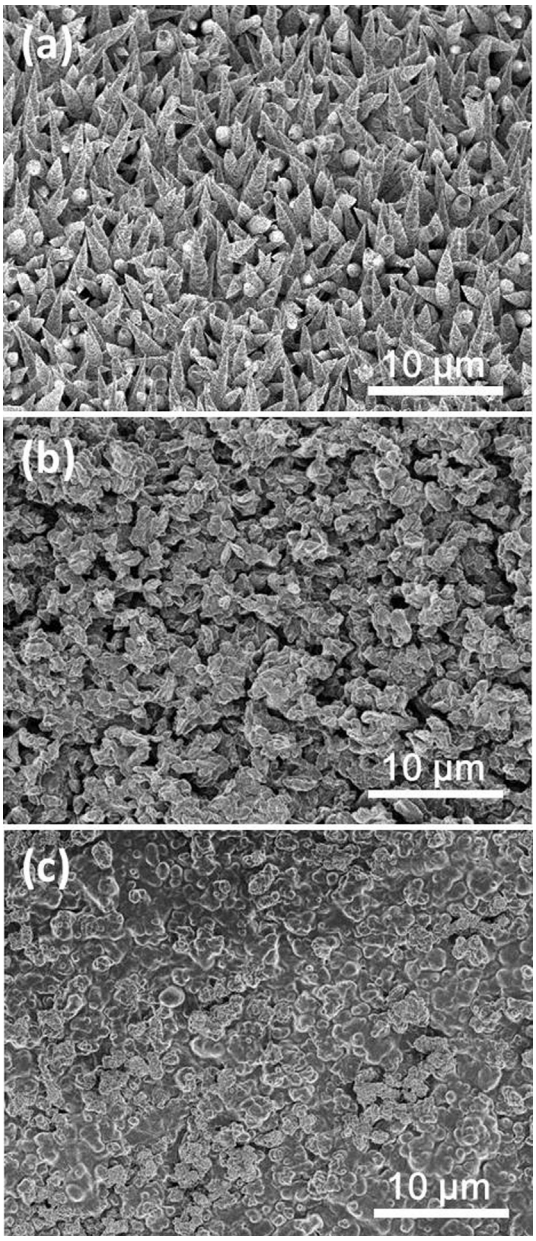

Fig. 1. SEM image of (a) electrodeposited Cu microcones array structure substrate. (b) Si–O–C composites thick film deposited on a microcones array substrate. (c) Si–O–C composites thick film anode after charge–discharge cycles.

For electrodeposition of the Si–O–C composite, the electrolytic solution containing 0.5 mol dm^{-3} $SiCl_4$ (Sigma–Aldrich) and 0.1 mol dm^{-3} tetrabuthylammonium perchlorate in propylene carbonate ($TBAClO_4$, Kanto Chemical/PC, Kishida, H_2O content less than 30 ppm) was prepared in dry air. The electrochemical cell equipped with a Li/Li^+ reference electrode, 4.0 cm^2 Cu microcone-arrays substrate as a working electrode, and Pt counter electrode was set up in Ar atmosphere. A constant potential of −2.4 V vs. Pt was applied to pass a charge of 8 C cm^{-2} for the deposition. The as-prepared Si–O–C composite thick film was rinsed by PC and dried in vacuum for 2 h. The depth profile of elements from the results of X-ray photoelectron spectroscopy supported homogeneous distribution of Si, O, and C elements in the deposit, with the weight ratio of Si, O, and C being ca. 60, 20, and 20 wt.%, respectively. The origin of oxygen and carbon is the decomposition products of the organic electrolyte during the electrodeposition process [15,16].

The resultant Si–O–C composite anode of a Li battery was transferred into a three-electrode electrochemical cell containing 1.0 mol dm^{-3} lithium perchlorate ($LiClO_4$) in PC – ethylenecarbonate (EC) (1:1 v/v) electrolyte solution (Kishida, H_2O content less than 20 ppm) and Li metal foils as both reference electrode and counter electrode. The cell was assembled inside an Ar-filled glove box and used for galvanostatic cycling with potential limitation and impedance measurement. The gravimetric capacity of the Si-based composite electrode was calculated according to the weight of silicon in the composites obtained from inductively coupled plasma (ICP) analysis. The galvanostatic cycling with potential limitation were performed with a Bio-Logic VMP3 multichannel galvanostat–potentiostat at 0.1 mA cm^{-2} (0.1 C-rate). Electrochemical impedance spectra were taken with a potentiostat and frequency response analyzer (Solartron, 1400) over the frequency range from 1 MHz to 0.01 Hz with AC amplitude of 10 mV. The EIS data were fitted with Microsoft Excel Solver to reach the minimum value of the sum of the difference between the acquired experimental complex impedance data and the impedances calculated with the equivalent circuit using the parameters obtained by fitting for each frequency. In our model the fitting error is usually less than 1%.

The surface morphologies of the microcone-arrayed current collector and the Si–O–C composite film were observed by means of field emission scanning electron microscopy (FESEM, Hitachi, S-4800). The cross sectional images were obtained by the high resolution transmission electron microscopy (HRTEM, JEOL, 2100F). The TEM specimen was prepared by focused ion beam (FIB, SEIKO, SMI2050).

3. Results and discussion

3.1. General characterization of the Si–O–C composite electrode

Fig. 1 (a) shows a typical scanning electron microscopy (SEM) image of the Cu microcones array current collector fabricated by electroless plating. The deposited Cu layer exhibits a rough surface with serried and uniform cones distribution. The average height of Cu cones is about 5 μm and the mean base diameter is estimated to be 1 μm. After the deposition of Si–O–C composite, as shown in Fig. 1 (b), the microcones array structure was completely covered by submicrometer clusters with large amount of voids. However, the surface morphology became less porous after the charge/discharge cycles, as shown in Fig. 1 (c). This phenomenon is more obvious by comparing the cross sectional TEM images of the electrode before and after cycling which are shown in Fig. 2 (a) and (b). Both of the electrodes before and after cycling appear in seamless contact between the film and Cu microcones array substrate. It is clear from

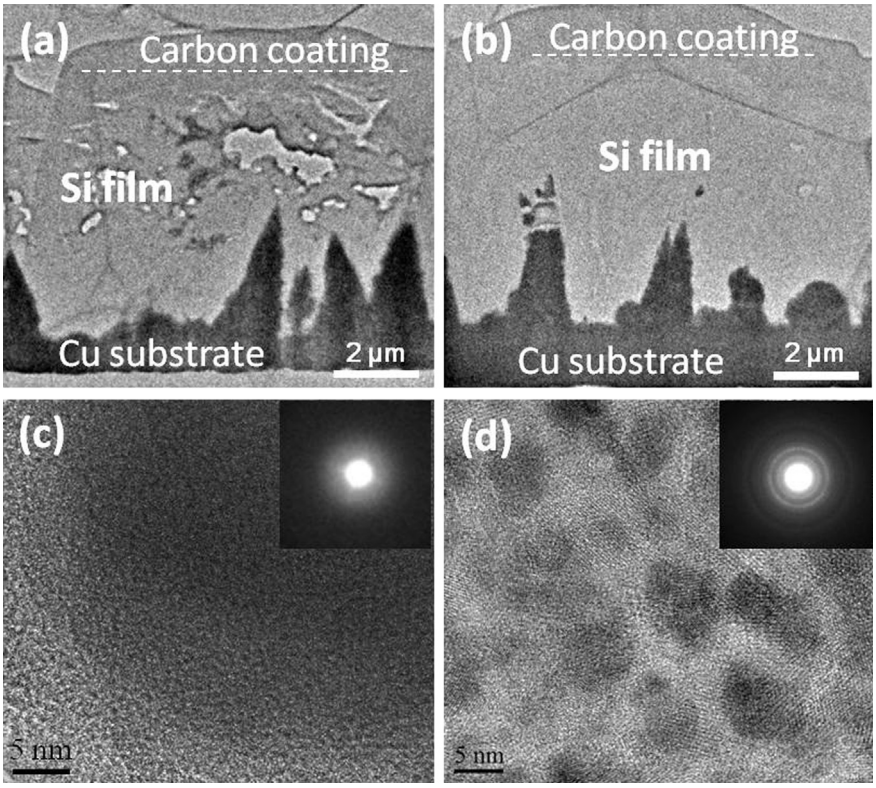

Fig. 2. TEM image of the Si–O–C composite thick film deposited on Cu microcones array substrate. (a) low magnification of as-deposited thick film; (b) low magnification of the thick film anode after cycling; (c) high resolution image of the as-deposited thick film and (d) high resolution image of the Si–O–C film after cycling. The insets in (c) and (d) are the diffraction pattern obtained by TEM.

the cross sectional images that the thickness of the Si film doesn't increase too much during cycling, but the quantity and the size of the voids obviously decrease. This is because the large volume change during the lithiation/delithiation cycles results in the reorganization of the deposit. The crystallinity of the Si–O–C composite film was investigated by *ex-situ* HR-TEM. The as deposited Si film was suggested to be amorphous structure (Fig. 2 (c)) and it was confirmed by the diffraction pattern shown in the inset of Fig. 2 (c). However, in Fig. 2 (d), crystallites a few nanometers in size are observed in the HR-TEM image of the composite film after cycling. The crystallinity was slightly increased after 100 cycles (inset of Fig. 2 (d)). The lattice parameters of these nano-crystallites are close to those of silicon dioxide and lithium silicate [26]. This result is corresponded with our previously reported results [16]. Meanwhile, there are some amorphous regions among these hazy lattice strips, which were assumed to be Si.

Fig. 3 shows the typical voltage profile of the Si–O–C composite anode. The lithiation potential shows a sloping profile below 0.30 V vs Li+/Li, being consistent with lithiation behavior of amorphous Si [27]. The potentionstatic differential capacity–voltage curve derived from the voltage profile (inset of Fig. 3) enables a more detailed understanding on the delithiation process. Two adjacent peaks are found at 0.32 V and 0.46 V vs Li/Li^+ indicating the phase transition from a-$Li_{3.75}Si$ to a-Li_xSi then to a-Si [28].

3.2. Equivalent circuit and typical fitting parameters

The electrode morphology described in Fig. 2 (a) is a thick film with larger or smaller pores that can be partially filled by the liquid electrolyte. It is similar to a composite electrode comprised of particles with different sizes. Several equivalent circuits have been reported to describe the situation, from the classical Randles circuit to more complex systems built by several sub-circuits [23]. In Fig. 4, we present the equivalent circuit which was used for simulating the experimental Nyquist plot of the Si–O–C composite thick film electrode measured at different potential. The circuit includes: a solution resistance (R_s) and an inductive component, which consists of inductor and resistor (L and R_l) related to the wiring between the electrode attached to the current collector and the measuring equipment; two RC parallel elements in series describing the SEI film on the surface (R_f and CPE_f) and lithium ion charge transfer at interface (R_{ct} and CPE_{ct}), respectively; and Warburg impedance for solid state diffusion of lithium ions. The double

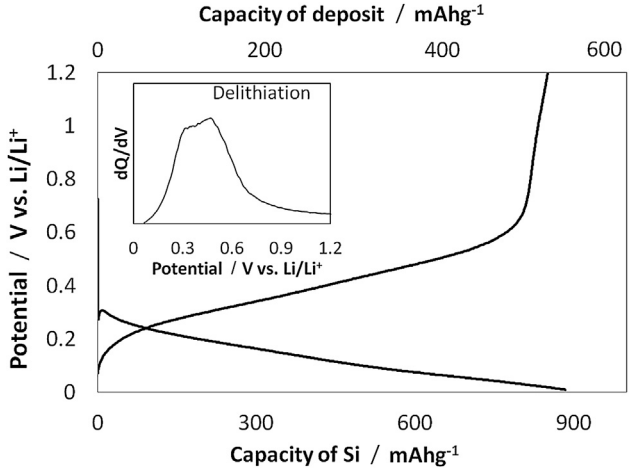

Fig. 3. Typical voltage profile of the Si–O–C composite anode. The inset shows the differential capacity–voltage curves for the delithiation process.

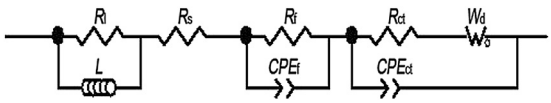

Fig. 4. The equivalent circuit used to model the impedance spectra in this study. Symbols of the equivalent circuit were expressed as follows: L, inductance of current collector and battery case; R_l, resistance of current collector; R_s, resistance of electrolyte and current collector; R_{ct}, interfacial charge transfer resistance; CPE_f and CPE_{ct} constant phase element of SEI and electrode surface layer; W_d, Warburg impedance.

layer capacitance has been replaced by a constant phase element (CPE) in our model because the Si–O–C composite film is not continuous and the sizes of the clusters are distributed around average values. The impedance of CPE can be expressed by Eq. (1):

$$Z_{CPE} = 1/\left((j\omega)^{pT}\right) \quad (1)$$

When $p = 1$, T has the unit of a capacitance "F cm^{-2}". Note that CPE_{ct} is not only the double layer capacitance at interface, but also includes the lithium intercalation capacitance in the active materials.

A typical fitting plot of this Si–O–C composite anode is illustrated in Fig. 5 with the data of the ac impedance responses measured at 0.3 V vs. Li/Li^+ during 1st delithiation (about 20% DOD). At very high frequencies (above 100 kHz), the spectrum exhibits an inductance response below the real axis, which is dominated by the contribution of the external cell connections and resistance of the electrolyte. No significant changes were observed in this frequency range throughout all the experiments. As the frequency decreases (between 100 kHz and 1 Hz), a smaller semicircle at high frequency and a larger semicircle at mid frequency are observed. This can be attributed to the presence of a passive SEI layer and the charge transfer resistance in parallel with the double layer capacitances. At low frequencies (below 1 Hz), the contribution from solid state diffusion is confirmed. In this frequency region the spectrum shows typical semi-finite diffusion behavior. Thus the finite space Warburg element was used for modeling. The diffusion impedance, Z_d, is defined by Eq. (2):

$$Z_d = R_d(j\omega\tau)^{-p}\coth(j\omega\tau)^p \quad (2)$$

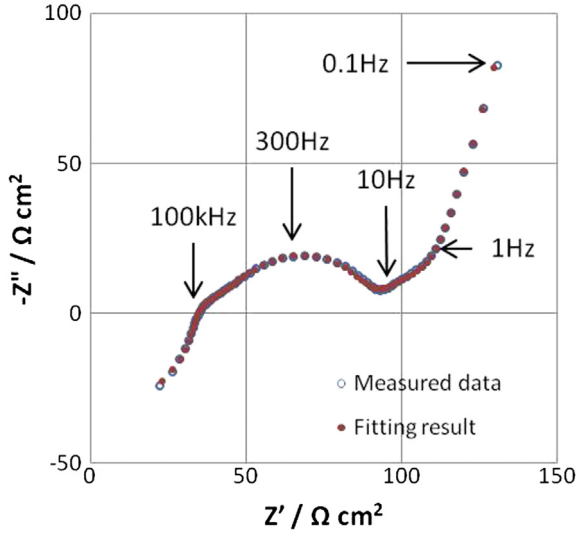

Fig. 5. Typical fitting plots of experimental impedance spectrum of this Si–O–C composites thick film electrode measured at discharge potential of 0.3 V vs. Li/Li^+, frequency range: 1 MHz to 0.1 Hz, signal amplitude 10 mV.

where j is $\sqrt{-1}$, ω is angular frequency, τ is the time constant, $p = 0.5$ for the ideal finite-space behavior, and R_d is the diffusion resistance which can be calculated from the low-frequency limit of the real part of Z. As was discussed elsewhere [29], it may not appear straightforward to use this relationship, since such inhomogeneous distribution of the film's thickness will result in a rather complicated situation for Li-ion diffusion; while in the thick parts of the Si–O–C film a semi-infinite diffusion takes place, in thin parts equilibrium may be reached. Here, we just discuss the change trend of R_d.

The dotted curve in Fig. 5 shows the impedance calculated using the equivalent circuit in Fig. 4. The fitting parameters obtained from the equivalent circuit are presented in Table 1. Note that the resistance of inductive component R_l is a negative value which is theoretically used for fitting and does not exist as a discrete component, thus the parameters of outer component are not shown in the table. Besides, a satisfactory agreement between the experimental and simulated Nyquist plots in the low-frequency domain was achieved by using unfixed $p = 0.42$, instead of $p = 0.5$, for the ideal finite space Warburg element.

3.3. Impedance dependence on the depth of delithiation

The change in composition of the Si electrode is described in terms of the depth of discharge (DOD) during lithium extraction. The electrodes were lithiated to 0.01 V vs. Li/Li^+ by constant current (CC) with 50 μA cm^{-2} and were maintained at 0.01 V until the current density fell below 1 μA cm^{-2}, then delithiated at the current density of 50 μA cm^{-2}. During the delithiation, the current was stopped at different potentials to obtain LIBs with different DODs. Each EIS spectrum was collected at the end of the corresponding CC–CV step after waiting 1 h for relaxation at the open circuit voltage (OCV) condition. Fig. 6 shows the Nyquist plot of the measured impedances at different discharge potentials and frequency ranges. All of these impedance spectra measured at different DOD can be fitted by the equivalent circuit shown in Fig. 4, except for impedance spectrum obtained at very high DOD (discharge above 1.0 V). The dependence of fitted resistance parameters on discharge potential is shown in Fig. 7. Except for the abrupt increase of R_d at high DOD, the main contribution to the total resistance of delithiation can be attributed to R_{ct} change. With an increase of discharge potential from 0.2 V, the charge-transfer resistance decreased, and showed the minimum value at about 0.3 V, then slightly increased from 0.3 V to 0.5 V, with accelerated rise at potentials above 0.5 V. This is very similar to the behavior of the carbonaceous electrode reported by A. Funabiki [18]. The increase of R_{ct} from the discharge potential of 0.3 V–0.2 V may be attributed to volume expansion of the active materials which block the diffusion path of the lithium ion into the electrode. It was also reported that the phase transformation of crystalline $Li_{14}Si_{15}$ to amorphous Si during discharge above 0.2 V will result in a decrease

Table 1
Typical fitting parameters.

Electrolyte	R_s	32.1 Ω
SEI	R_f	19.9 Ω cm^2
	CPE_f-T	1.9E-04
	CPE_f-p	0.5
Charge transfer	R_{ct}	34.9 Ω cm^2
	CPE_{ct}-T	2.7E-05
	CPE_{ct}-p	0.9
Diffusion	R_d of W_d	65.7 Ω cm^2
	T of W_d	1.2
	p of W_d	0.42

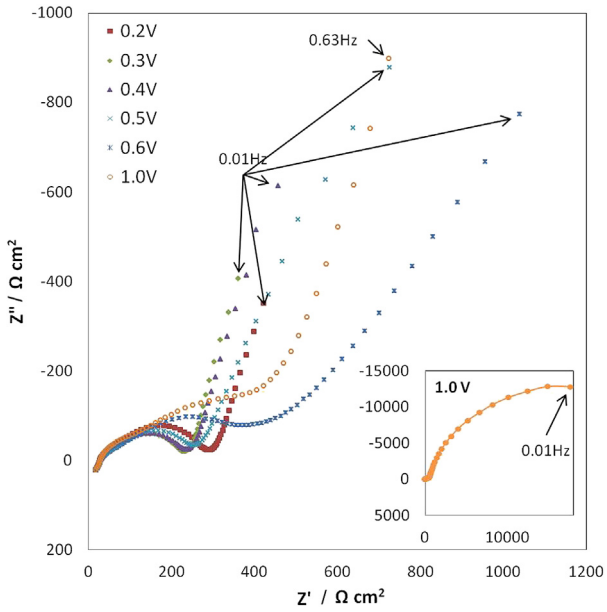

Fig. 6. Nyquist plot of Si–O–C composite thick film anode with several different discharge potential. The lowest frequency impedances (at 0.01 Hz) are indicated by arrows, except for the one measured at 1.0 V, shown as the inset.

of charge transfer resistance [22]. On the other hand, the increase of R_{ct} at high DOD may be attributed to the decrease of the electronic conductivity inside the electrode, due to the transformation of lithium silicate to amorphous silicon. A gradual decrease of SEI resistance R_f is also observed, in agreement with already reported results for amorphous silicon thin films and has been attributed to the mild dissolution of the SEI during discharge [24]. R_s, which is not shown in the figure, remains almost constant during the discharge process. The significant increase of R_d indicates that the lithium diffusion in active materials becomes very difficult at high DOD. But the reason for this change is not clearly understood. In fact, the low frequency impedance behavior at very high DOD (above 1.0 V) is quite different from that measured at other DODs. As shown in the inset of Fig. 6, the impedance at the frequency of diffusion appears as a part of an arc instead of the semi-infinite diffusion behavior. This behavior was explained as the contribution of structure/phase transformation in the Si thick film electrode [23]. However, we can't make a conclusion on the mechanism of kinetics change simply with EIS analysis, and more direct evidence is needed.

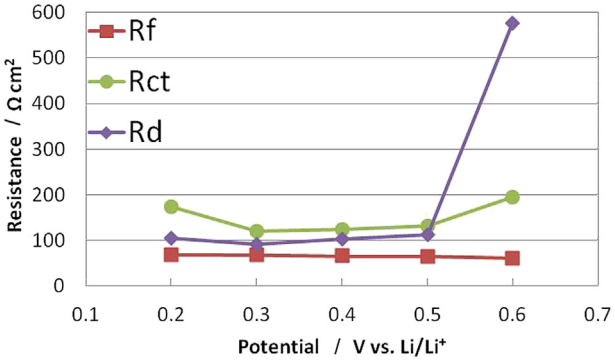

Fig. 7. Variation of charge transfer resistance (R_{ct}), SEI resistance (R_f) and diffusion resistance (R_d) with level of discharge, obtained by fitting of experimental impedance spectra measured after 200 charge–discharge cycles.

3.4. Impedance change after charge–discharge cycles

Fig. 8 reveals the capacity value of the Si–O–C composite thick film anode under a loading current of 100 μA cm^{-2}, which corresponds to a value of 0.2 in C-rate. In the initial stage, the composite exhibited a high value of discharge capacity above 1000 mAh g^{-1} of Si. After the 10th cycle, this value decreases to 900 mAh g^{-1} of Si, and then returns to 1000 mAh g^{-1} again after 50 cycles. Finally, it gradually decreases while the discharge capacity is kept at a value higher than 800 mAh g^{-1} of Si for more than 200 cycles. The Coulombic efficiency increases from 80% to 97% during the initial 5 cycle, and then slowly increases to 98.5% during the following 200 cycles.

To better understand the capacity fading mechanism of these Si–O–C composite thick film electrodes, Fig. 9 shows the Nyquist plot at the discharge potential of 0.3 V after the indicated number of cycles. They have generally the same features as illustrated in Fig. 5. By fitting the impedance data using the equivalent circuit in Fig. 4, the change in resistance parameters during 200 cycles at the same DOD (discharge potential of 0.3 V) are shown in Fig. 10. No change of R_s (not shown in the figure) was observed during cycling. The degradation of the electrolyte can be neglected because of enough amount of electrolyte by using a beaker type cell. As shown in the figure, the resistance of the surface film, R_f, rapidly increased over the first five cycles, indicating the formation of SEI film on the electrode. Compared to the change trend of R_f and the Coulombic efficiency shown in Fig. 8, we can conclude that the formation of a passive layer on the electrode may be responsible for the initial irreversible capacity. During the following cycling, the gradual increase of R_f indicates the slow growth of the SEI film. On the contrary, the resistance of the diffusion R_d decreased during the first 5 cycles, and then slowly increased during the following 200 cycles. The diffusion resistance is related to the diffusion coefficient and the diffusion length. The decrease of R_d during the first 3 cycles may be attributed to a decrease of diffusion length due to the decrease of film thickness, which was confirmed by SEM in our previous work [16], while the slow increase of R_d may be attributed to the film density increase after long time cycling.

The charge transfer R_{ct} increased dramatically during the first 10 cycles, which is consistent with the capacity decrease during the first 10 cycles. An abrupt decrease at the 50th cycle may be due to cracking in the composite film, leading to the formation of electronic pathways and/or ionic pathways in the anode matrix. The cracking of the Si film has been observed by SEM in our previous study [13]. After 50 cycles, the charge transfer resistance gradually increases until 100 cycles and remains almost constant for following cycles, which demonstrates that the cracked thick film has not disintegrated and degraded with the Cu microcones array current collector sticking to the active materials tightly. Thus the

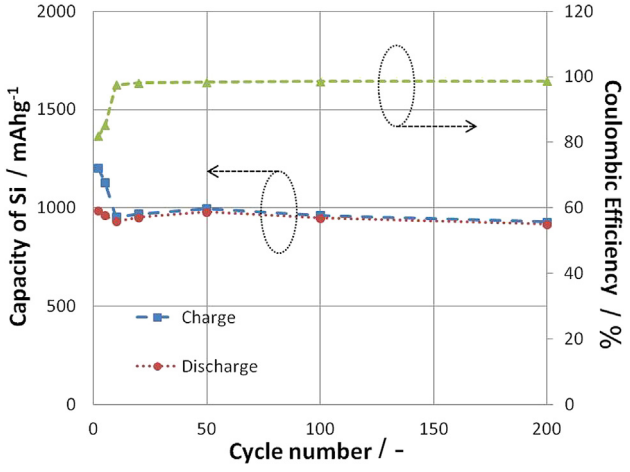

Fig. 8. Plot of electrode capacity and coulombic efficiency with the number of charge–discharge cycles.

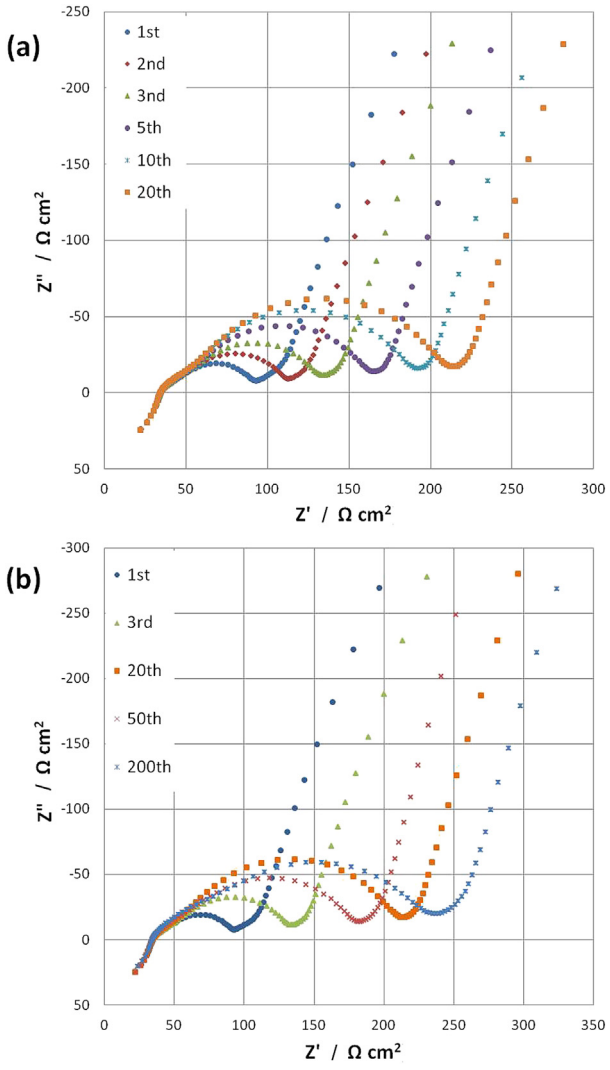

Fig. 9. Typical Nyquist plot of the battery at the discharge voltage of 0.3 V with different number of cycles.

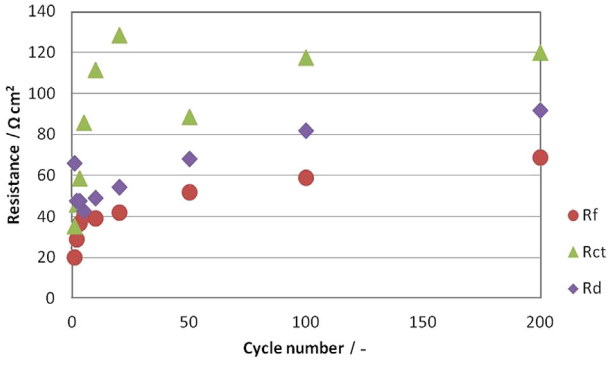

Fig. 10. Plots of charge transfer resistance (R_{ct}), SEI resistance (R_f) and diffusion resistance (R_d) as function of cycle number, obtained by fitting of experimental impedance spectra measured at discharge potential of 0.3 V vs. Li/Li^+.

long term degradation of the Si composite thick film electrode is due to the slow growth of the surface film as well as the increase of the diffusive resistance during cycling.

4. Conclusions

In summary, a microcone array structure supported silicon composite film fabricated by electrodeposition was studied by electrochemical impedance spectroscopy. The morphology and structure analysis of the electrode show that the as-deposited Si–O–C composite film becomes less porous after cycling, and the transition from amorphous to nano-crystalline has been observed. From the EIS result, the change of charge transfer resistance is the main contribution to the total resistance change during discharge. The abrupt increase of the diffusion resistance is not explained very well by the present model. The kinetics of this Si–O–C composite electrode cannot be simply concluded by EIS study due to lack of direct evidence. The impedance evolution of this Si–O–C thick film anode during charge/discharge cycles has also been studied by EIS technique. The initial irreversible capacity during the first 5 cycles is mainly attributed to the formation of the SEI film on the electrode surface, while the long term degradation of the electrode may be due to the slow growth of the SEI film as well as the increase of the electrode density during cycling. A significant decrease of charge transfer resistance after 50 cycles is also observed, which may be attributed to the cracking in the electrode. The EIS technique has been shown as an effective tool to investigate the mechanism of capacity fading of this Si–O–C composite thick film anode.

Acknowledgments

This work was supported by “Research & Development Initiative for Scientific Innovation of New Generation Batteries” from the New Energy and Industrial technology Development Organization of Japan.

References

[1] H.G. Zhang, X.D. Yu, P.V. Braun, Nat. Nanotechnol. 6 (2011) 277–281.
[2] X.L. Ji, S. Evers, R. Black, L.F. Nazar, Nat. Commun. 2 (2011).
[3] J.Y. Huang, L. Zhong, C.M. Wang, J.P. Sullivan, W. Xu, L.Q. Zhang, S.X. Mao, N.S. Hudak, X.H. Liu, A. Subramanian, H.Y. Fan, L.A. Qi, A. Kushima, J. Li, Science 330 (2010) 1515–1520.
[4] Y. Yao, K.F. Huo, L.B. Hu, N.A. Liu, J.J. Ha, M.T. McDowell, P.K. Chu, Y. Cui, ACS Nano 5 (2011) 8346–8351.
[5] T. Song, J.L. Xia, J.H. Lee, D.H. Lee, M.S. Kwon, J.M. Choi, J. Wu, S.K. Doo, H. Chang, W. Il Park, D.S. Zang, H. Kim, Y.G. Huang, K.C. Hwang, J.A. Rogers, U. Paik, Nano Lett. 10 (2010) 1710–1716.
[6] J.T. Yin, M. Wada, K. Yamamoto, Y. Kitano, S. Tanase, T. Sakai, J. Electrochem. Soc. 153 (2006) A472–A477.
[7] U. Kasavajjula, C.S. Wang, A.J. Appleby, J. Power Sources 163 (2007) 1003–1039.
[8] J. Graetz, C.C. Ahn, R. Yazami, B. Fultz, Electrochem. Solid State Lett. Electrochem. Solid State Lett. 6 (2003) A194–A197.
[9] J.H. Ryu, J.W. Kim, Y.E. Sung, S.M. Oh, Electrochem. Solid State Lett. Electrochem. Solid State Lett. 7 (2004) A306–A309.
[10] M. Green, E. Fielder, B. Scrosati, M. Wachtler, J. Serra Moreno, Electrochem. Solid State Lett. Electrochem. Solid State Lett. 6 (2003) A75–A79.
[11] X.L. Chen, K. Gerasopoulos, J.C. Guo, A. Brown, C.S. Wang, R. Ghodssi, J.N. Culver, ACS Nano 4 (2010) 5366–5372.
[12] R.A. Huggins, J. Power Sources 81 (1999) 13–19.
[13] T. Hang, H. Nara, T. Yokoshima, T. Momma, T. Osaka, J. Power Sources 222 (2013) 503–509.
[14] T. Momma, S. Aoki, H. Nara, T. Yokoshima, T. Osaka, Electrochem. Commun. 13 (2011) 969–972.
[15] H. Nara, T. Yokoshima, T. Momma, T. Osaka, Energy Environ. Sci. 5 (2012) 6500–6505.
[16] H. Nara, T. Yokoshima, M. Otaki, T. Momma, T. Osaka, Electrochim. Acta 107 (2013) 1–8.
[17] J.C. Guo, A. Sun, X.L. Chen, C.S. Wang, A. Manivannan, Electrochim. Acta 56 (2011) 3981–3987.
[18] A. Funabiki, M. Inaba, Z. Ogumi, J. Power Sources 68 (1997) 227–231.
[19] H. Li, X.J. Huang, L.Q. Chen, J. Power Sources 81 (1999) 340–345.
[20] N. Dimov, K. Fukuda, T. Umeno, S. Kugino, M. Yoshio, J. Power Sources 114 (2003) 88–95.
[21] N. Dimov, S. Kugino, M. Yoshio, Electrochim. Acta 48 (2003) 1579–1587.
[22] Y.M. Kang, J.Y. Go, S.M. Lee, W.U. Choi, Electrochem. Commun. 9 (2007) 1276–1281.
[23] R. Ruffo, S.S. Hong, C.K. Chan, R.A. Huggins, Y. Cui, J. Phys. Chem. C. 113 (2009) 11390–11398.
[24] Y.M. Lee, J.Y. Lee, H.T. Shim, J.K. Lee, J.K. Park, J. Electrochem. Soc. 154 (2007) A515–A519.
[25] W.J. Zhang, Z.Y. Yu, Z. Chen, M. Li, Mater. Lett. 67 (2012) 327–330.
[26] Q. Sun, B. Zhang, Z.W. Fu, Appl. Surf. Sci. 254 (2008) 3774–3779.
[27] J.C. Li, A.K. Dozier, Y.C. Li, F.Q. Yang, Y.T. Cheng, J. Electrochem. Soc. 158 (2011) A689–A694.
[28] H. Liu, L.B. Hu, Y.S. Meng, Q. Li, Nanoscale 5 (2013) 10376–10383.
[29] M.D. Levi, Z. Lu, D. Aurbach, Solid State Ionics 143 (2001) 309–318.